Received: 11 June 2019 | Revised: 2 August 2019 | Accepted: 14 August 2019

DOI: 10.1002/dta.2683

RESEARCH ARTICLE

WILEY

Toxicokinetics and analytical toxicology of the abused opioid U-48800 — in vitro metabolism, metabolic stability, isozyme mapping, and plasma protein binding

Tanja M. Gampfer[1] | Lilian H.J. Richter[1] | Jan Schäper[2] | Lea Wagmann[1] | Markus R. Meyer[1]

[1] Department of Experimental and Clinical Toxicology, Institute of Experimental and Clinical Pharmacology and Toxicology, Center for Molecular Signaling (PZMS), Saarland University, Homburg, Germany

[2] State Bureau of Criminal Investigation Bavaria, Munich, Germany

Correspondence
Markus R. Meyer, Department of Experimental and Clinical Toxicology, Institute of Experimental and Clinical Pharmacology and Toxicology, Center for Molecular Signaling (PZMS), Saarland University. Homburg, Germany.
Email: markus.meyer@uks.eu

Abstract

Due to the risk of new synthetic opioids (NSOs) for human health, the knowledge of their toxicokinetic characteristics is important for clinical and forensic toxicology. U-48800 is an NSO structurally non-related to classical opioids such as morphine or fentanyl and offered for abuse. As toxicokinetic data of U-48800 is not currently available, the aims of this study were to identify the in vitro metabolites of U-48800 in pooled human liver S9 fraction (pS9), to map the isozymes involved in the initial metabolic steps, and to determine further toxicokinetic data such as metabolic stability, including the in vitro half-life ($t_{1/2}$), and the intrinsic (CL_{int}) and hepatic clearance (CL_h). Furthermore, drug detectability studies in rat urine should be done using hyphenated mass spectrometry. In total, 13 phase I metabolites and one phase II metabolite were identified. *N*-Dealkylation, hydroxylation, and their combinations were the predominant metabolic reactions. The isozymes CYP2C19 and CYP3A4 were mainly involved in these initial steps. CYP2C19 poor metabolizers may suffer from an increased U-48800 toxicity. The in vitro $t_{1/2}$ and CL_{int} could be rated as moderate, compared to structural related compounds. After administration of an assumed consumer dose to rats, the unchanged parent compound was found only in very low abundance but three metabolites were detected additionally. Due to species differences, metabolites found in rats might be different from those in humans. However, phase I metabolites found in rat urine, the parent compound, and additionally the *N*-demethyl metabolite should be used as main targets in toxicological urine screening approaches.

KEYWORDS

LC–HRMS/MS, metabolic stability, new synthetic opioids, pooled human liver S9 fraction

1 | INTRODUCTION

New psychoactive substances (NPS) can be subdivided in different groups such as stimulants, synthetic cannabinoids, hallucinogens, or new synthetic opioids (NSOs). Although the total number of emerging NPS has slowly decreased in recent years, more and more NSOs have appeared on the market.[1-3] They are usually sold via the Internet and only limited pharmacological and toxicological data are available. Several cases of acute intoxications and deaths were described recently and clearly underline the health risks associate with an NSO abuse.[4,5]

Investigations on the toxicokinetic characteristics of NSOs are of great importance regarding analytical questions but also for a thorough general risk assessment, particularly in terms of simultaneous drug intake.

The NSO U-48800 [trans-2-(2,4-dichlorophenyl)-N-2-(dimethylamino)cyclohexyl)-N-methylacetamide, monohydrochloride] appeared in 2017 for the first time on the market in seized material.[6] Together with its regioisomer U-51754 (methene-U-47700), which was also described as an NSO,[7,8] it belongs to the so-called U-drugs and is structurally non-related to classical opioids such as morphine and fentanyl.[6,9] Both chemical structures are given in Figure 1. U-48800 receptor affinity studies were not yet performed, but based on the analogy to U-51754, comparable pharmacological effects are likely.[6,7] Due to a higher affinity to the κ-receptor in comparison to the μ-receptor, analgesia with fewer unwanted pharmacological effects such as respiratory depression could be expected. Solimini et al recently reviewed the pharmacotoxicology of non-fentanyl-derived NSOs and found U-48800 available as a "research chemical" of the opioid analgesic class to replace U-47700 and that conventional drug tests do not detect such compounds.[10] Due to the growing number of acute intoxication cases, they encouraged pharmacological, toxicological, and forensic research on these compounds to provide effective detection methods, amongst others.

Toxicokinetic studies including metabolism of compounds similar to U-48800 were for example published for AH-7921.[11] Wohlfarth et al studied the metabolic stability and in vitro metabolism of AH-7921 and confirmed findings in a urine sample.[11] They identified 12 metabolites in vitro and 11 in urine with the demethyl and bisdemethyl metabolites being the most abundant in vitro. However, such studies are essential for developing e. g. urinary screening procedures. Since authentic human samples are often unavailable and studies of drugs of abuse in human are not feasible for ethical reasons, alternative in vivo models, such as rats, have to be used. However, species differences might occur. Detailed toxicokinetic data including metabolism of U-48800 had not yet been described. Therefore, the aims of the present study were to elucidate its in vitro metabolic stability, including in vitro half-life ($t_{1/2}$), intrinsic clearance (CL_{int}), hepatic clearance (CL_h), its qualitative metabolism, involvement of single monooxygenases in the initial steps, as well as its plasma protein binding (PPB). Finally, the detectability of U-48800 intake should be shown in rat urine samples after administration of an assumed consumer's dose.

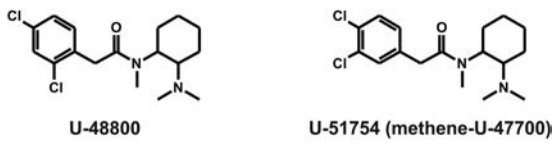

FIGURE 1 Chemical structures of U-48800 and its isomer U-51754 (methene-U-47700)

2 | EXPERIMENTAL

2.1 | Chemicals, reagents, and enzymes

U-48800 was provided for research purposes by the State Bureau of Criminal Investigation Bavaria (Munich, Germany). A stock solution was prepared in methanol (1 mg/mL). Trimipramin-d_3 was from LGC (Wesel, Germany). Isocitrate, isocitrate dehydrogenase, superoxide dismutase, 3′-phosphoadenosine-5'phosphosulfate (PAPS), S-(5′-adenosyl)-L-methionine (SAM), dithiothreitol (DTT), reduced glutathione (GSH), magnesium chloride ($MgCl_2$), potassium dihydrogenphosphate (KH_2PO_4), dipotassium hydrogenphosphate (K_2HPO_4), and tris hydrochloride were obtained from Sigma Aldrich (Taufkirchen, Germany) and $NADP^+$ from Biomol (Hamburg, Germany). Acetonitrile (LC–MS grade), methanol (LC–MS grade), ammonium formate (analytical grade), formic acid (LC–MS grade), and all other reagents and chemicals (analytical grade) were obtained from VWR (Darmstadt, Germany). The creatinine immunoassays and the PIA^2 device were from Protzek Diagnostik (Lörrach, Germany). The baculovirus-infected insect cell microsomes (Supersomes) containing 1 nmol/mL of human cDNA-expressed cytochrome P450 (CYP) isoforms CYP1A2, CYP2A6, CYP2B6, CYP2C8, CYP2C9, CYP2C19, CYP2D6, CYP2E1 (2 nmol/mL), CYP3A4, CYP3A5 (2 nmol/mL), flavin-containing monooxygenase (FMO) 3 (5 mg/mL), pS9 (20 mg microsomal protein/mL), UGT reaction mixture solution A (25mM UDP-glucuronic acid), and UGT reaction mixture solution B (250mM Tris HCl, 40mM MgCl2, and 125 μg/mL alamethicin) were obtained from Corning (Amsterdam, Netherlands). After delivery, the enzymes and pS9 were thawed at 37°C, aliquoted, snap-frozen in liquid nitrogen, and stored at −80°C until use.

2.2 | Pooled human liver S9 fraction incubation for identification of phase I and II metabolites and investigation of metabolic stability

U-48800 was incubated with pS9 (2 mg microsomal protein/mL) in accordance to a previous publication with minor modifications.[12] First, 25 μg/mL alamethicin (UGT reaction mixture solution B), 90mM phosphate buffer (pH 7.4), 2.5mM Mg^{2+}, 2.5mM isocitrate, 0.6mM NADP+, 0.8 U/mL isocitrate dehydrogenase, 100 U/mL superoxide dismutase were preincubated for 10 minutes at 37°C. Thereafter, 2.5mM UDP-glucuronic acid (UGT reaction mixture solution A), 40 μM PAPS, 1.2mM SAM, 1mM DTT, 10mM GSH, and 2.5 μM substrate were

added. The amount of organic solvent was below 1%.[13] All given concentrations are concentrations in the final incubation mixture (final volume: 300 µL).

Reactions were started by adding U-48800. The maximum incubation time was 360 minutes and 30 µL aliquots were taken after 1, 15, 30, 45, 60, 75, 90, 180, and 360 minutes. Reactions were terminated by addition of 10 µL ice-cold acetonitrile containing trimipramin-d_3 (5 µM) as internal standard (IS). Afterwards, the tubes were cooled for 30 minutes at −20°C, centrifuged at 18,407 × g for 2 minutes, the supernatants transferred to autosampler vials, and analyzed by liquid chromatography coupled to high-resolution tandem mass spectrometry (LC–HRMS/MS). Blank incubation (without substrate) and control incubation (without pS9) were done to confirm the absence of interfering compounds and to identify not metabolically formed compounds. All incubations were performed in duplicate.

Metabolic stability was evaluated by substrate depletion. Statistical analysis was done using GraphPad Prism 5.00 (GraphPad Software, San Diego, CA, USA). The natural logarithm of the area ratio of the analyte to the IS was plotted versus incubation time (1–90 minutes). The slope of the linear regression was used to calculate in vitro half-life. A t-test was performed to confirm that the $\ln[\text{peak area ratio}]_{\text{initial}}$ of the remaining analyte was not significantly different from the ln[peak area ratio] of the control incubation without pS9. The following settings were used: unpaired; two-tailed; significance level, 0.05; confidence intervals, 99%.

Following equations were used according to Baranczewski and Obach[14,15]:

$$t_{1/2} = \frac{\ln 2}{k\ (\text{min})} \tag{1}$$

$$\ln[\text{peak area ratio}]_{\text{remaining}} = \ln[\text{peak area ratio}]_{\text{initial}} - k \times t \tag{2}$$

$$\text{CL}_{\text{int}} = \frac{\ln 2}{t_{1/2}(\text{min})} \times \frac{[\text{V}]_{\text{incubation}}\ (\text{ml})}{[\text{P}]_{\text{incubation}}(\text{mg})} \times \frac{[\text{Liver}]\ (\text{g})}{[\text{BW}]\ (\text{kg})} \times \text{SF}\left(\frac{\text{mg}}{\text{g}}\right) \tag{3}$$

$$\text{CL}_{\text{h}} = \frac{\text{Q} \times f_u \times \text{CL}_{\text{int}}}{\text{Q} + f_u \times \text{CL}_{\text{int}}} \tag{4}$$

$$\text{CL}_{\text{h}} = \frac{\text{Q} \times \text{CL}_{\text{int}}}{\text{Q} + \text{CL}_{\text{int}}} \tag{5}$$

(well-stirred model with[4] and without[5] free fraction in plasma)

$$\text{CL}_{\text{h}} = \text{Q} \times \left(1 - e^{\left(\frac{-f_u \times \text{CL}_{\text{int}}}{\text{Q}}\right)}\right) \tag{6}$$

$$\text{CL}_{\text{h}} = \text{Q} \times \left(1 - e^{\left(\frac{-\text{CL}_{\text{int}}}{\text{Q}}\right)}\right) \tag{7}$$

(parallel tube model with[6] and without[7] free fraction in plasma)

with k = slope of the linear regression fit, $t_{1/2}$ = in vitro half-life, CL_{int} = intrinsic clearance, [V]incubation = incubation volume = 0.3, [P]incubation = amount of S9 protein in the incubation = 0.6, [Liver][BW] = liver weight normalized by body weight = 26,[16] and SF = scaling factor S9 protein per gram of liver = 121,[17] CL_{h} = hepatic clearance, Q = hepatic blood flow rate in human = 20 mL/min/kg,[18] f_u = free fraction in plasma.

2.3 | Isozyme mapping

Monooxygenases activity screening was performed in accordance to a previous study with minor modifications.[19] U-48800 (2.5 µM) was incubated with CYP1A2, CYP2A6, CYP2B6, CYP2C8, CYP2C9, CYP2C19, CYP2D6, CYP2E1, CYP3A4, CYP3A5 (50 pmol/mL each), or FMO3 (0.25 mg protein/mL) for 30 minutes at 37°C. All given concentrations are concentrations in the final incubation mixture (final volume: 250 µL). Furthermore, the incubation mixtures contained 90mM phosphate buffer (pH 7.4), 5mM Mg^{2+}, 5mM isocitrate, 1.2mM NADP+, 0.5 U/mL isocitrate dehydrogenase, and 200 U/mL superoxide dismutase. For incubations with CYP2A6 or CYP2C9, phosphate buffer was replaced by 90mM tris buffer, according to the manufacturer's recommendation. The reactions were initiated by addition of the respective enzyme and terminated after 30 µL aliquots were taken at 1, 5, 10, 15, 20, 25, and 30 minutes by addition of 10 µL ice-cold acetonitrile. Afterwards, the samples were centrifuged at 18 407 × g for 5 minutes, the supernatants transferred to autosampler vials, and analyzed by LC –HRMS/MS. Blank incubation with CYP2E1 and without substrate and a negative control without enzyme were done to confirm the absence of interfering compounds and to identify not metabolically formed compounds. All incubations were performed in duplicate.

2.4 | Plasma protein binding studies

Two-chambered Centrifree devices from Merck (Darmstadt, Germany) were used for determination of PPB and f_u. According to published procedures,[20,21] 450 µL fresh human plasma samples were spiked with 50 µL U-48800 methanolic solution (final concentration: 0.5 µM) and incubated for 30 min at 37°C (n = 3). Before filtration, a 100 µL aliquot (global approach, GA) was transferred to a new reaction tube. After filtration for 35 minutes at 37°C and 1,600 × g, 100 µL of the ultrafiltrate (UF) was also transferred to a new reaction tube. All reactions were terminated by addition of 50 µL ice-cold acetonitrile containing trimipramin-d_3 (2.5 µM) as IS. Afterwards, samples were cooled for 30 minutes at −20°C, centrifuged for 2 minutes at 18,407 × g, transferred into autosampler vials and analyzed by LC –HRMS/MS. Calculation of lipophilicity was done using ChemDraw Professional 16.0.1.4 (PerkinElmer, Waltham, MA, USA). The PPB was calculated using the following equations:

$$f_u = \frac{\text{peak area ratio}\left(\frac{U48800_{UF}}{IS_{UF}}\right)}{\text{peak area ratio}\left(\frac{U48800_{GA}}{IS_{GA}}\right)} \tag{8}$$

$$\text{PPB},\ \% = (1 - f_u) \times 100 \tag{9}$$

2.5 | Rat urine samples

As reported earlier,[22] drug detectability studies were performed using rat urine samples from male Wistar rats (Charles River, Sulzfeld, Germany) for toxicological diagnostic reasons according to the corresponding German animal protection law. The rat dosage was based on a common consumer U-47700 dosage (http://drugs.tripsit.me/) due to unavailable consumer data of U-48800. After a single 0.6 mg/kg body mass dose administration, urine and faces were collected separately over 24 hours. Blank urine was collected before drug administration to confirm the absence of interfering compounds. Creatinine was measured in blank urine and after administration by an immunoassay. Samples were stored at −20°C until use.

2.6 | Sample preparation for drug detectability studies in rat urine

Urine precipitation (UP) was done in accordance to Wissenbach et al.[23] A volume of 200 µL rat urine was precipitated with 1 mL ice-cold acetonitrile, shaken for 2 minutes, and centrifuged at 18 407 × g for 2 minutes. The supernatant was evaporated to dryness at 70°C under nitrogen stream, and reconstituted in 100 µL eluent mixture A and B (50:50 v/v, Section 2.7). The samples were analyzed using both the mass spectrometry settings described in Section 2.7 and by standard urine screening approach (SUSA) in switching mode and without inclusion list with minor modifications.[24]

2.7 | LC–HRMS/MS conditions

A Thermo Fisher Scientific (TF, Dreieich, Germany) Dionex UltiMate 3000 RS pump consisting of a degasser, a quaternary pump, and an UltiMate autosampler, coupled to a TF Q-Exactive Plus system equipped with a heated electrospray ionization (HESI)-II source were used. A mass calibration was done according to the manufacturer's recommendations using external mass calibration prior to analysis. Injection volume was 1 µL for all samples. Gradient elution was performed according to a previous study[24] on a TF Accucore PhenylHexyl column (100 mm x 2.1 mm, 2.6 µm). The mobile phases consisted of 2mM aqueous ammonium formate containing formic acid (0.1%, v/v, pH 3, eluent A) and 2mM ammonium formate solution with acetonitrile: methanol (1:1, v/v), water (1%, v/v), and formic acid (0.1%, v/v, eluent B). The initial flow rate was set to 500 µL/min (0–10 minutes) and 800 µL/min (10–13.5 minutes). The gradient was stepped as follows: 0–1.0 minute hold 99% A, 1–10 minute to 1% A, 10–11.5 minute hold 1% A, and 11.5–13.5 minute hold 99% A. The HESI-II source conditions were as follows: heater temperature, 320°C; ion transfer capillary temperature, 320°C; spray voltage, 4.0 kV; ionization mode, positive; sheath gas, 60 arbitrary units (AU); auxiliary gas, 10 AU; sweep gas, 0 AU; and S-lens RF level, 50.0. Mass spectrometry was performed using full scan data and a subsequent data-dependent acquisition (DDA) with priority to mass-to-charge ratios (*m/z*) of parent compounds and their expected metabolites. The settings for full scan data acquisition were the following: resolution, 35 000; microscans, 1; automatic gain control (AGC) target, 1e6; maximum injection time (IT), 120 ms; and scan range, *m/z* 50–750. The settings for the DDA mode with an inclusion list of U-48800 and its expected metabolites were as follows: option "pick others," enabled; dynamic exclusion, 5 seconds; resolution, 17500; microscans, 1; isolation window, 1.0 *m/z*; loop count, 5; AGC target, 2e5; maximum IT, 250 ms; high collision dissociation cell with stepped normalized collision energy, 17.5, 35.0, 52.5; exclude isotopes, on; spectrum data type, profile; and underfill ratio, 1%. The inclusion list contained *m/z* values of likely formed metabolites such as *N*-dealkyl and hydroxy metabolites (phase I) as well as sulfates, glucuronides, methoxy metabolites (phase II), and combinations thereof. ChemSketch 2010 12.01 (ACD/Labs, Toronto, Canada) was used to draw structures of hypothetical metabolites and to calculate the exact masses. TF Xcalibur Qual Browser software version 2.2 SP1.48 (TF, Dreieich, Germany) was used for data handling. The following automated peak integration settings were used: peak detection algorithm, INCOS; baseline window, 40; area noise factor, 5; and peak noise factor, 10.

3 | RESULTS AND DISCUSSION

3.1 | In vitro metabolic stability, half-life, intrinsic clearance, and hepatic clearance

Metabolic stability was determined by a substrate depletion assay using a low protein concentration of 2 mg/mL to minimize nonspecific protein binding.[14] Furthermore, a low substrate concentration (2.5 µM) was used to ensure a linear metabolite formation during incubation time. The t-test confirmed no significant difference between the natural logarithms of the peak area ratios of incubations after 1 minute and control incubations.

Metabolic stability data are summarized in Table Table S1 in the Supporting Information. The calculated in vitro $t_{1/2}$ of 54.5 minutes was longer than previously published for the structurally related compound AH-7921.[11] The CL_{int} was calculated to be 20 mL/min/kg, which can be considered as intermediate in accordance to McNaney et al.[25] To predict human hepatic clearance (CL_h), two different models (well-stirred, parallel tube) were used. Calculation using the well-stirred model including f_u yielded 1.4 mL/min/kg and parallel tube model 1.5 mL/min/kg. In the case of basic substances, the calculated in vitro CL_h values are in higher agreement with in vivo clearance data without considering the PPB.[15] The calculated CL_h without considering f_u was 10.0 mL/min/kg based on the well-stirred model and 12.6 mL/min/kg based on the parallel tube model. The results obtained by the two models were comparable within the with and without considering f_u groups. Within one model, the clearance was much lower considering f_u than without f_u. This would lead to an underestimation of the measured in vivo clearance.

3.2 | Identification of in vitro metabolites

Twelve phase I metabolites were tentatively identified in pS9 or CYP isozyme incubations by comparison of their MS^2 spectra to the MS^2 spectrum of U-48800. The measured accurate masses of precursor ion (PI) and characteristic fragment ions (FI), relative intensities in MS^2, calculated exact masses, elemental compositions, mass deviation errors, and retention times (RT) of U-48800 and its metabolites are listed in Table S2. The metabolites were sorted by increasing mass and RT. Only calculated exact masses will be used in the following chapter for discussion of in vitro phase I metabolites. The MS^2 spectra of U-48800 and the most abundant metabolites in pS9 and in monooxygenase activity studies are given in Figure 2. The MS^2 spectra of all other metabolites are given in Figure S1. The metabolic pathways detected in all investigated models are given in Figure 3.

The MS^2 spectrum of U-48800 (PI at *m/z* 343.1338), showed FI at *m/z* 298.0759, which originated from the separation of the tertiary amine. A cleavage of the cyclohexyl ring led to FI at *m/z* 218.0133, followed by FI at *m/z* 158.9762 generated after the amide cleavage. FI at *m/z* 112.1120 contained the cyclohexyl ring coupled with the methylated amine. The cyclohexyl ring was represented by the FI at *m/z* 81.0698. M2 (PI at *m/z* 329.1181), formed by *N*-demethylation of the tertiary amine, had the same FIs as the parent compound. M1 (PI at *m/z* 315.1025), originated from *N,N*-bisdemethylation of the tertiary amine, was characterized by the FI at *m/z* 298.0759, which was identical with the FI in the MS^2 spectrum of the parent compound. M8, M11, and M12 (PI at *m/z* 359.1287) were hydroxylated at the cyclohexyl ring indicated by the FI at *m/z* 110.0964, which consisted of the cyclohexyl ring with the primary amine shifted by two hydrogen after loss of water. M9, M10 and M13 (PI at *m/z* 359.1287) were formed by hydroxylation of the phenyl ring characterized by the FI at *m/z* 234.0083, which corresponded to the FI at *m/z* 218.0133 shifted by an oxygen. The *N*-demethyl hydroxy metabolite M4 (PI at *m/z* 345.1131) showed the same FI pattern as the corresponding hydroxy metabolites (M9, M10, M13). M5 and M6 (PI at *m/z* 345.1131) are the corresponding *N*-demethyl hydroxy isomers of M8, M11, M12 and their FIs are in accordance with each other. M3 (PI at *m/z* 331.0974) originated from a hydroxylation at the cyclohexyl ring and *N,N*-bisdemethylation at the tertiary amine, which was identified by the FI at *m/z* 114.0913, which corresponded to the FI at *m/z* 128.1069 altered in one CH_2 group. The absence of interfering compounds was confirmed by blank incubations. M2 was also identified in negative control incubations, but with much lower intensity than in the pS9 and single isozyme incubations, most probably due to degradation processes during storage.

M3, M4, M5, M6, M8, M9, M10, and M13 were only identified in CYP isozyme incubations. This was most probably due to higher total CYP concentrations in incubations with recombinant CYP isozymes in comparison to pS9 incubations. However, as pS9 represents the relative CYP isozyme amounts within the human liver, the metabolites which were only detected in CYP isozyme incubations may be expected to be minor metabolites in vivo. Another reason could be suppression or enhancement effects in the different matrices, which could not be excluded.

3.3 | Isozyme mapping

All metabolites previously identified in pS9 and eight additional metabolites were found in the isozymes incubations in total (Table S3). The *N*-demethylation, the most abundant step in vitro, was catalyzed by several isozymes (CYP2B6, CYP2C19, CYP2D6, CYP3A4, CYP3A5). Furthermore, CYP2C19 was involved in all other metabolic steps. M3, M4, M8, M10, and M13 were only identified in CYP2C19, while M5 and M9 was formed only in CYP3A4 incubations. Besides the *N,N*-demethyl metabolite (M1), the *N*-demethyl-hydroxy metabolite (M5), and the hydroxy metabolite (M9), the formation of the *N*-demethyl-hydroxy isomer (M6) and the hydroxy isomer (M11) was catalyzed by CYP3A4. Thus, CYP2C19 and CYP3A4 are the predominant isozymes involved in the metabolism of U-48800. The changes in the U-48800 amount and the formation rates of the three most abundant metabolites in pS9, CYP2C19, and CYP3A4 incubations are given in Figure 4. Inhibition of one or both of these two isozymes, for example by drug–drug interactions or varying activity due to different CYP2C19 expression levels may cause an increased U-48800 concentration and thus toxicity.

3.4 | Determination of plasma protein binding

As classical ultrafiltration may have the non-specific binding as disadvantages compared to equilibrium dialysis,[26] the used filtration membrane consisted of regenerated cellulose, which was shown to avoid this issue.[27] Free fraction of U-48800 represents unbound drug (f_u) and was calculated to be 0.078, which resulted in a PPB of 92% (log P value of 3.4). Amongst other factors, for example ionization state, there is a high correlation between lipophilicity and PPB.[28,29] It is expected that a PPB over 70% would have significant effects on the pharmacokinetics and pharmacodynamics such as lower clearance.[30] However, this effect will depend on the elimination route and/or active transport into the hepatocytes,[31] which were not part of this study. Therefore, further studies are encouraged.

3.5 | Detectability of metabolites in rat urine

The only metabolite that could be automatically identified in urine by automated SUSA was M7. Therefore, a more sensitive but targeted approach was additionally used to allow the identification of more than one biomarker. The metabolic pathways in rats are shown in Figure 3. Two phase I (M5, M7) and one phase II metabolite (M14) could be detected using the settings described in Section 2.7, whereas M5 has already been identified in vitro. M7 (PI at *m/z* 345.1131) is the N-demethyl-hydroxy isomer of M4 with identical MS^2 pattern. The MS^2 spectrum of M14 (PI at *m/z* 375.1236) is given in Figure S2. M14 was formed by *N*-demethylation of the

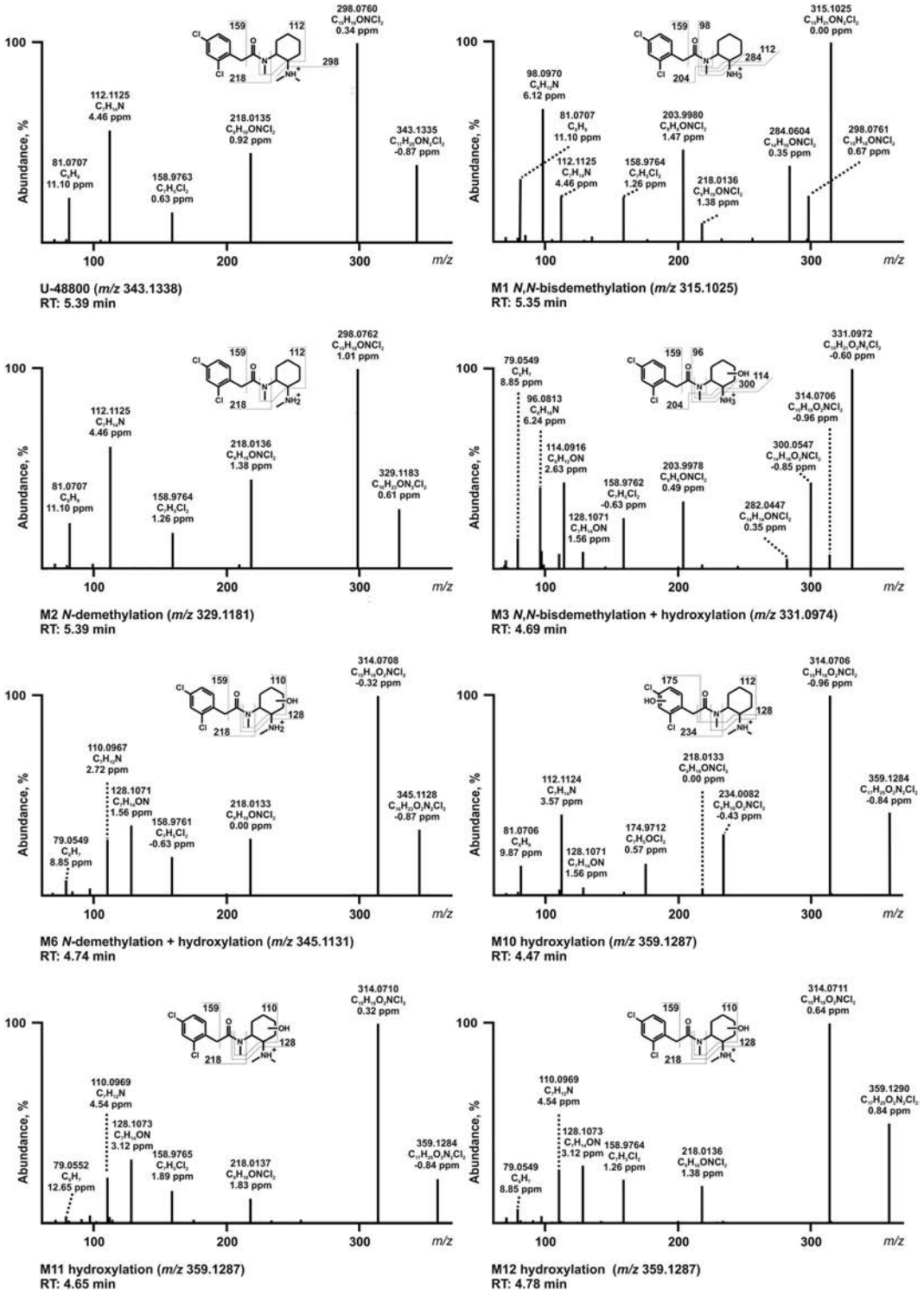

FIGURE 2 MS^2 spectra of U-48800 and seven proposed major phase I metabolites in pooled human S9 fraction (pS9) and monooxygenases incubations sorted by precursor ions and retention time (RT)

tertiary amine and dihydroxylation at the phenyl ring followed by methylation of one hydroxy group, characterized by the FI at *m/z* 344.0814, which showed a shift of a CH_3 and NH_2 moiety. In comparison to the listed metabolites, the unchanged parent compound was only found at a very low abundance in urine. By comparing these findings in rat urine to findings in human urine of structural related compounds, except the *N*-demethyl-hydroxy-methoxy metabolite, the two phase I metabolites were identified.[11,32] Therefore, analytical procedures should include the parent compound and the described phase I metabolites. Additionally, the *N*-demethyl metabolite only identified in vitro should be considered due to the high abundance in the investigated human urine.[32] The absence of

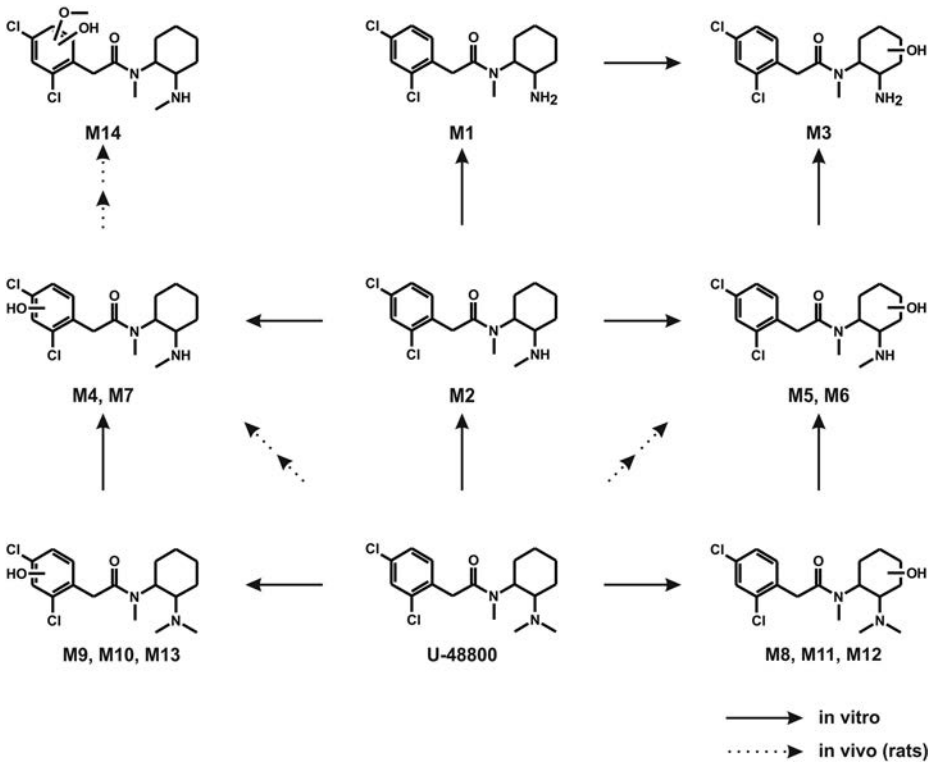

FIGURE 3 In vitro and in vivo (rats) metabolic pathways of U-48800

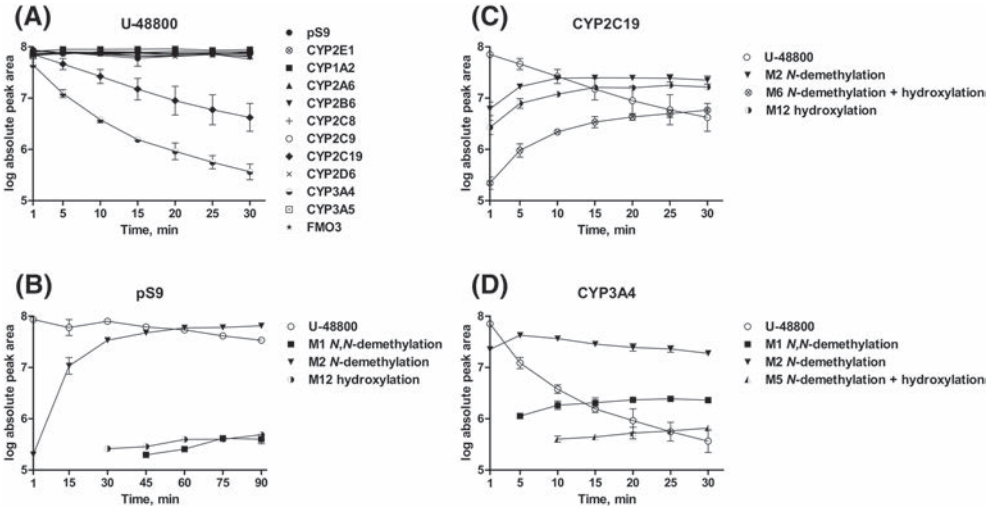

FIGURE 4 Changes of the U-48800 amount in pS9 and isozymes in A and incubations and the formation rates of the most abundant metabolites compared to parent compound in B, pS9; C, CYP2C19; and D, CYP3A4. Logarithm of the absolute peak areas were plotted against time (min)

interfering compound was confirmed by analysis of blank urine. Creatinine values of blank urine and after dose administration were 76 mg/dL and 87 mg/dL.

4 | CONCLUSIONS

The present study describes the in vitro toxicokinetics and in vivo detectability of the NSO U-48800. In total, 14 metabolites were tentatively identified. *N*-dealkylation, hydroxylation, and combinations thereof were the main metabolic reactions. The CYP isozyme mapping revealed the predominant involvement in the initial steps of CYP2C19 and CYP3A4. CYP2C19 polymorphisms could therefore lead to increased drug concentrations and subsequent toxicity cannot be excluded. Predicted CL_{int} and $t_{1/2}$ is rated as intermediate in comparison to another NSO. Detection of a U-48800 intake in human urine should be possible by LC–HRMS/MS-based urine screening approaches. Both phase I metabolites found in rat urine, the parent

compound, and additionally the most abundant in vitro metabolite *N*-demethyl-U48800 should be considered as main targets.

ACKNOWLEDGEMENTS

The authors like to thank Matthias J. Richter, Gabriele Ulrich, and Armin A. Weber for their support.

CONFLICT OF INTEREST

The authors declare that there is no conflict of interest.

ORCID

Markus R. Meyer https://orcid.org/0000-0003-4377-6784

REFERENCES

1. UNODC. Global SMART Update Volume 17. 2017.
2. EMCDDA. European Drug Report 2018. Publications of of the European Union. 2018. http://www.emcdda.europa.eu/system/files/publications/8585/20181816_TDAT18001ENN_PDF.pdf.
3. Fentanils and synthetic cannabinoids: driving greater complexity into the drug situation. An update from the EU Early Warning System. EMCDDA; 2018. http://www.emcdda.europa.eu/system/files/publications/8870/2018-2489-td0118414enn.pdf. Accessed 10/07/2018.
4. Muller D, Neurath H, Neukamm MA, et al. New synthetic opioid cyclopropylfentanyl together with other novel synthetic opioids in respiratory insufficient comatose patients detected by toxicological analysis. *Clin Toxicol (Phila)*. 2019;57(9):806-812.
5. Garneau B, Desharnais B, Beauchamp-Dore A, Lavallee C, Mireault P, Lajeunesse A. Challenges related to three cases of fatal intoxication to multiple novel synthetic opioids. *J Anal Toxicol*. 2019;n/a. https://doi.org/10.1093/jat/bkz018 epub ahead of print
6. Sharma KK, Hales TG, Rao VJ, NicDaeid N, McKenzie C. The search for the "next" euphoric non-fentanil novel synthetic opioids on the illicit drugs market: current status and horizon scanning. *Forensic Toxicol*. 2019;37(1):1-16.
7. Beardsley PM, Zhang Y. Synthetic opioids. *Handb Exp Pharmacol*. 2018;252:353-381.
8. Fabregat-Safont D, Carbon X, Ventura M, et al. Updating the list of known opioids through identification and characterization of the new opioid derivative 3,4-dichloro-N-(2-(diethylamino)cyclohexyl)-N-methylbenzamide (U-49900). *Sci Rep*. 2017;7(1):6338.
9. Loew G, Lawson J, Toll L, Frenking G, Berzetei-Gurske I, Polgar W. Structure activity studies of two classes of beta-amino-amides: the search for kappa-selective opioids. *NIDA Res Monogr*. 1988;90:144-151.
10. Solimini R, Pichini S, Pacifici R, Busardo FP, Giorgetti R. Pharmacotoxicology of non-fentanyl derived new synthetic opioids. *Front Pharmacol*. 2018;9:654.
11. Wohlfarth A, Scheidweiler KB, Pang S, et al. Metabolic characterization of AH-7921, a synthetic opioid designer drug: in vitro metabolic stability assessment and metabolite identification, evaluation of in silico prediction, and in vivo confirmation. *Drug Test Anal*. 2016;8(8):779-791.
12. Richter LHJ, Maurer HH, Meyer MR. New psychoactive substances: studies on the metabolism of XLR-11, AB-PINACA, FUB-PB-22, 4-methoxy-alpha-PVP, 25-I-NBOMe, and meclonazepam using human liver preparations in comparison to primary human hepatocytes, and human urine. *Toxicol Lett*. 2017;280:142-150.
13. Chauret N, Gauthier A, Nicoll-Griffith DA. Effect of common organic solvents on in vitro cytochrome P450-mediated metabolic activities in human liver microsomes. *Drug Metab Dispos*. 1998;26(1):1-4.
14. Baranczewski P, Stanczak A, Sundberg K, et al. Introduction to in vitro estimation of metabolic stability and drug interactions of new chemical entities in drug discovery and development. *Pharmacol Rep*. 2006;58(4):453-472.
15. Obach RS. Prediction of human clearance of twenty-nine drugs from hepatic microsomal intrinsic clearance data: an examination of in vitro half-life approach and nonspecific binding to microsomes. *Drug Metab Dispos*. 1999;27(11):1350-1359.
16. Davies B, Morris T. Physiological parameters in laboratory animals and humans. *Pharm Res*. 1993;10(7):1093-1095.
17. Houston JB, Galetin A. Methods for predicting in vivo pharmacokinetics using data from in vitro assays. *Curr Drug Metab*. 2008;9(9):940-951.
18. Boxenbaum H. Interspecies variation in liver weight, hepatic blood flow, and antipyrine intrinsic clearance: extrapolation of data to benzodiazepines and phenytoin. *J Pharmacokinet Biopharm*. 1980;8(2):165-176.
19. Wagmann L, Meyer MR, Maurer HH. What is the contribution of human FMO3 in the N-oxygenation of selected therapeutic drugs and drugs of abuse? *Toxicol Lett*. 2016;258:55-70.
20. Fung EN, Chen YH, Lau YY. Semi-automatic high-throughput determination of plasma protein binding using a 96-well plate filtrate assembly and fast liquid chromatography-tandem mass spectrometry. *J Chromatogr B Analyt Technol Biomed Life Sci*. 2003;795(2):187-194.
21. Mardal M, Gracia-Lor E, Leibnitz S, Castiglioni S, Meyer MR. Toxicokinetics of new psychoactive substances: plasma protein binding, metabolic stability, and human phase I metabolism of the synthetic cannabinoid WIN 55,212-2 studied using in vitro tools and LC-HR-MS/MS. *Drug Test Anal*. 2016;8(10):1039-1048.
22. Welter J, Kavanagh P, Meyer MR, Maurer HH. Benzofuran analogues of amphetamine and methamphetamine: studies on the metabolism and toxicological analysis of 5-APB and 5-MAPB in urine and plasma using GC-MS and LC-(HR)-MS(n) techniques. *Anal Bioanal Chem*. 2015;407(5):1371-1388.
23. Wissenbach DK, Meyer MR, Remane D, Weber AA, Maurer HH. Development of the first metabolite-based LC-MS(n) urine drug screening procedure-exemplified for antidepressants. *Anal Bioanal Chem*. 2011;400(1):79-88.
24. Helfer AG, Michely JA, Weber AA, Meyer MR, Maurer HH. Orbitrap technology for comprehensive metabolite-based liquid chromatographic-high resolution-tandem mass spectrometric urine drug screening - exemplified for cardiovascular drugs. *Anal Chim Acta*. 2015;891:221-233.
25. McNaney CA, Drexler DM, Hnatyshyn SY, et al. An automated liquid chromatography-mass spectrometry process to determine metabolic stability half-life and intrinsic clearance of drug candidates by substrate depletion. *Assay Drug Dev Technol*. 2008;6(1):121-129.
26. Barre J, Chamouard JM, Houin G, Tillement JP. Equilibrium dialysis, ultrafiltration, and ultracentrifugation compared for determining the plasma-protein-binding characteristics of valproic acid. *Clin Chem*. 1985;31(1):60-64.
27. Kratzer A, Kees F, Dorn C. Unbound fraction of fluconazole and linezolid in human plasma as determined by ultrafiltration: impact of membrane type. *J Chromatogr B Analyt Technol Biomed Life Sci*. 2016;1039:74-78.
28. Fauber BP, Rene O, de Leon Boenig G, et al. Reduction in lipophilicity improved the solubility, plasma-protein binding, and permeability of tertiary sulfonamide RORc inverse agonists. *Bioorg Med Chem Lett*. 2014;24(16):3891-3897.

29. Zhivkova ZD. Quantitative structure - pharmacokinetics relationships for plasma protein binding of basic drugs. *J Pharm Sci*. 2017;20(1):349-359.

30. Lindup WE, Orme MC. Clinical pharmacology: plasma protein binding of drugs. *Br Med J (Clin Res Ed)*. 1981;282(6259):212-214.

31. Howard ML, Hill JJ, Galluppi GR, McLean MA. Plasma protein binding in drug discovery and development. *Comb Chem High Throughput Screen*. 2010;13(2):170-187.

32. Krotulski AJ, Mohr ALA, Papsun DM, Logan BK. Metabolism of novel opioid agonists U-47700 and U-49900 using human liver microsomes with confirmation in authentic urine specimens from drug users. *Drug Test Anal*. 2018;10(1):127-136.

SUPPORTING INFORMATION

Additional supporting information may be found online in the Supporting Information section at the end of the article.

How to cite this article: Gampfer TM, Richter LHJ, Schäper J, Wagmann L, Meyer MR. Toxicokinetics and analytical toxicology of the abused opioid U-48800 — in vitro metabolism, metabolic stability, isozyme mapping, and plasma protein binding. *Drug Test Anal.* 2019;11:1572–1580. https://doi.org/10.1002/dta.2683